Nanoscale

ARTICLE

Determining Molecular Orientation via Single Molecule SERS in a Plasmonic Nano-gap

Received 00th January 20xx,
Accepted 00th January 20xx

DOI: 10.1039/x0xx00000x

www.rsc.org/

Addison R L Marshall,[a] Jamie Stokes, [a] Francesco. N. Viscomi,[a] John E. Proctor,[a,b] Johannes Gierschner,[c] Jean-Sebastien Bouillard,*[a,d,e] and Ali M Adawi *[a,d]

In this work, plasmonic nano-gaps consisting of a silver nanoparticle coupled to an extended silver film have been fully optimized for single molecule Surface-Enhanced Raman Scattering (SERS) spectroscopy. The SERS signal was found to be strongly dependent on the particle size and the molecule orientation with respect to the field inside the nano-gap. Using Finite Difference Time Domain (FDTD) simulations to complement the experimental measurements, the complex interplay between the excitation enhancement and the emission enhancement of the system as a function of particle size were highlighted. Additionally in conjunction with Density Functional Theory (DFT), the well defined field direction in the nano-gap enables to recover the orientation of individual molecules.

Introduction

Plasmonics, relying on the coupling of photons with collective oscillations in the delocalized sea of electrons in metallic nanostructure, has proved to be a rapidly growing field of interest in recent years.[1] Combining key advantages directly linked to their nature, such as high field confinement, strong field enhancement, polarization and spectral selectivity, plasmonic systems are a promising route for many applications in fields as diverse as optoelectronics,[2, 3] information technology,[4, 5] life sciences and sensing.[6] Coupling plasmonic resonances with Raman spectroscopy constitutes an essential pillar of Surface Enhanced Raman Scattering (SERS) techniques, a powerful tool for material analysis,[7, 8] providing detailed, nonintrusive information on the molecular fingerprint of a target analyte down to the single molecule level.[9–14]

Conventional Raman spectroscopy provides detailed information about the molecular structure and conformation. When interacting with matter, light is predominantly elastically scattered in a process known as Rayleigh scattering. A small proportion of the light can however be inelastically scattered as energy is lost or gained through interaction with molecular vibrational or rotational levels. This inelastic scattering can be understood as the annihilation or creation of a quantum vibronic or a rotation excitation in the molecule, resulting in a red- or blue-shift in frequency of the scattered photons known as Stokes/anti-Stokes scattering respectively.[15–17] Raman spectroscopy provides a very powerful, non-invasive technique for material studies, however, it is limited by low Raman cross sections ~10^{-26}cm^2 [18] and ~10^{-29} cm^2 for single molecules[19] (equivalent to quantum yields of 10^{-6}-10^{-8} [20]). It is therefore fundamentally necessary to enhance this factor in order to detect trace quantities of materials.

SERS directly utilises the strong field enhancements achievable with plasmonics to overcome the small scattering cross sections linked to Raman processes. The narrow spectral width of vibrational Raman bands, and the relatively large spectral bandwidths of plasmonic resonances combine to make SERS a highly versatile sensing tool. Enhancement factors of the orders of 10^{7-8} [21] have been reported and detection of materials down to single molecule levels has been proven on numerous occasions.[9–14, 16, 21–23]

By bringing metallic nanostructures in close proximity to one another it is possible to generate highly confined regions of electromagnetic field[24] arising from the coupling of plasmonic modes known as plasmon hybridization. This coupling can lead to large local field enhancements resulting in very high local field intensities, commonly known as hot spots, which are highly suited for SERS applications. Plasmonic nano-gaps, formed between a nanoparticle and a metallic film, allow for the simple generation of hot spots,[6, 25–40] and have been shown to produce the high field intensities necessary to successfully observe Raman signal from single molecules.[33, 35, 37, 40] Albeit, in the vast majority of studies, emphasis is put on either observing single molecule SERS regime with very little information are gained on the molecular conformation of the target analyte or on the near-field enhancement in the nano-gap region. However, since most experimental configurations rely on the detection of the Raman signal in the far-field, the system's efficiency to couple to the far-field must also be taken into account. Understanding the complex interplay between the near-field excitation enhancements, molecular orientation and the far-field emission enhancements is an essential prerequisite for the development of fully optimised plasmonic devices for SERS applications.

[a] School of Mathematics and Physical Sciences, University of Hull, Cottingham road, HU6 7RX, UK. E-mail: a.adawi@hull.ac.uk and j.bouillard@hull.ac.uk
[b] Materials and Physics Research Group, School of Computing, Science and Engineering, University of Salford, Manchester M5 4WT, United Kingdom.
[c] Madrid Institute for Advanced Studies - IMDEA Nanoscience, Calle Faraday 9, Ciudad Universitaria de Cantoblanco, 28049 Madrid, Spain.
[d] G. W. Gray Centre for Advanced Materials, University of Hull, Cottingham road, HU6 7RX, UK.
[e] Department of Physics, King's College London, Strand, London, WC2R 2LS
† Footnotes relating to the title and/or authors should appear here.
Electronic Supplementary Information (ESI) available: [details of any supplementary information available should be included here]. See DOI: 10.1039/x0xx00000x

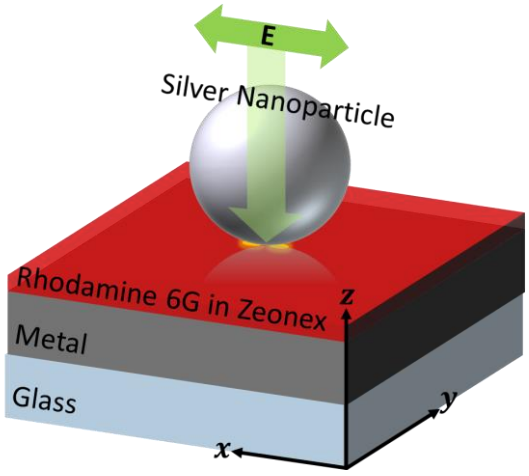

Fig. 1: Schematic representation of the SERS plasmonic nano-gap investigated in this work.

In this work the optical properties of plasmonic nano-gaps formed between a spherical silver nanoparticle and an extended silver film separated by a gap of width 5 nm (see Figure 1) are systematically investigated for SERS spectroscopy. The results reveal the intimate link between the near-field excitation enhancements and far-field emission enhancements for both the hybridized dipolar and quadrupolar modes of the nano-gaps as a function of the silver particle size. In particular, both finite difference time domain (FDTD) calculations and experimental measurements show that, in those nano-gaps, the SERS signal in the far-field is mainly associated with the hybridized dipolar mode of the nano-gap and strongly affected by the particle size. Finally, using an optimized nano-gap geometry, single molecule Raman sensitivity is demonstrated, enabling to determine the molecular orientation using a convolution of experimental single molecule SERS spectra and Density Functional Theory (DFT) calculations.

Experimental Section

Nano-gap fabrication

To fabricate the nano-gaps, firstly glass slides were thermally coated with a 100 nm layer of silver at a rate of ~0.2 nm.s^{-1}. Secondly a 5 nm dielectric film was spin-coated onto the metal film from a 1 mg.mL^{-1} solution of Zeonex polymer matrix (Zeon Chemicals Europe Ltd) in chloroform (Sigma-Aldrich) doped with the molecular dye Rhodamine 6G (Sigma-Aldrich) in concentrations ranging from 5×10^{-5} M to 2×10^{-7} M. To complete the nano-gaps, silver nanoparticles (Sigma-Aldrich, NanoComposix) suspended in a solution of ethanol at a concentration of 2.7×10^{6} particle.L^{-1} were spin-coated onto the Zeonex surface.

SERS measurements

The SERS measurements were performed using a custom-constructed Raman setup equipped with 532 nm wavelength laser line and 50× magnification objective lens with Numerical Aperture NA = 0.55 to excite and collect the Raman signal. The signal was then directed toward an iHR320 Horiba spectrometer where it was dispersed using a 1200 grating onto a nitrogen cooled Symphony CCD. To reject the Rayleigh scattering, two Kaiser holographic notch and super-notch filters centered at a wavelength of 532 nm were used.

Theoretical modelling

The electromagnetic response of the investigated nano-gaps were performed using Lumerical FDTD Solutions. Simulations used a 0.75 nm sub mesh surrounding the nanoparticle and nano-gap region. The boundaries of the structure utilize stretched coordinate perfect matching layer. Experimental data from Johnson and Christy[41] were used to describe the dielectric function of silver. Calculations were terminated when the fields decay below 1×10^{-5} of their original value. Absorption and scattering spectra were calculated using a total field scattered field (TFSF) configuration. Focused illumination was implemented using a Gaussian source consisting of the superposition of 200 plane waves. The far-field profile was calculated by transforming the near-field from the centre of the nano-gap using standard Lumerical far-field projection methods.
In the DFT calculations, Rhodamine 6G was fully optimized without symmetry constraints, resulting in a perpendicular arrangement between the phenyl and the xanthene moieties; thus, reoptimization was done under Cs symmetry. Geometry optimization and Raman spectrum were calculated at the DFT level of theory, employing the B3LYP functional and 6-311G* basis set, in chloroform using the polarizable continuum model (PCM) as defined in the Gaussian 09 program package.[42]

Results and Discussion

Electromagnetic contribution to SERS enhancement

In Raman scattering, the maximum available near-field enhancement due to electromagnetic mechanisms is proportional to the fourth power of the ratio of the overall electric field to the incident electric field at the location of the molecule, corresponding to enhancement at both the excitation and emission stages.[43] Additionally, consideration must be given to the orientation of the Raman active dipole moments, and therefore of the molecule, relative to the direction of the local enhanced electric field. By considering the enhancement of the incident field (excitation stage) and the increase in the optical density of states (emission stage) due to the present of the metallic nano-structure, the SERS enhancement can be expressed as:[24]

$$\boldsymbol{G} = \frac{|\boldsymbol{E}(\boldsymbol{\omega_0})|^2}{|\boldsymbol{E_0}(\boldsymbol{\omega_0})|^2}\left(\frac{|\hat{\boldsymbol{E}}.\hat{\boldsymbol{\mu}}|^2}{|\hat{\boldsymbol{E}}_{\boldsymbol{0}}.\hat{\boldsymbol{\mu}}|^2}\right)\frac{\boldsymbol{\rho}(\boldsymbol{\omega_1})}{\boldsymbol{\rho_0}(\boldsymbol{\omega_1})} = \boldsymbol{G_{ex}}\cdot\boldsymbol{S_{\mu}}\cdot\boldsymbol{G_{em}} \quad (1)$$

Where $\boldsymbol{E}_0$ is the incident electric field, $\boldsymbol{E}$ is the electric field at the location of the molecule, ω_0 is the frequency of the incident photon and ω_1 is the frequency of the photon after Raman scattering. $\hat{\boldsymbol{E}}_0$ and $\hat{\boldsymbol{E}}$ are the polarization directions of the incident electric field and the electric field at the molecule respectively, while $\hat{\boldsymbol{\mu}}$ refers to the orientation of molecular dipole associated with the Raman transition. ρ is the optical density of states in the presence of the plasmonic nano-gap and ρ_0 is the vacuum optical density of states. The term G_{ex} in Equation (1) represents the Raman enhancement due to excitation, G_{em} represents the Raman enhancement at the emission wavelengths due to the enhancements in the optical density of states in the presence of the plasmonic nano-gap and the

term S_μ represents the alignment of the transition dipole moment with respect to the local enhanced field.

Taking into account the random spatial localization of the analytes within the nano-gap, the excitation enhancement G_{ex} can be averaged out into an effective excitation enhancement $\langle G_{ex} \rangle$ expressed as the spatial average of G_{ex} over the cross sectional area of the nano-gap $a = \pi(D/2)^2$, with D the diameter of the nanoparticle:

$$\boldsymbol{G_{ex}} = \frac{1}{a}\int \frac{|E(\omega_0)|^2}{|E_0(\omega_0)|^2}\,\boldsymbol{da} \qquad (2)$$

The emission enhancement in the SERS signal can be written as

$$\boldsymbol{G_{em}} = \frac{\rho(\omega_0)}{\rho_0(\omega_0)} = \frac{P_{rad}}{P_0} \approx \frac{\sum_\theta E^2(\omega_1,\theta)}{\sum_\theta E_0^2(\omega_1,\theta)} \qquad (3)$$

Where P_{rad} and P_0 are the radiated Raman power to the far-field in the presence and in the absence of the plasmonic nano-gap. $\boldsymbol{E}^2(\omega_1,\theta)$ and $\boldsymbol{E}_0^2(\omega_1,\theta)$ are the far-field intensities as a function of emission angle θ in the presence and in the absence of the plasmonic nano-gap. From eq. 1, 2 and 3 the Raman enhancement figure of merit for a nano-gap system can then be written as:

$$\langle \boldsymbol{G(\lambda)} \rangle = \left(\frac{1}{a}\int \frac{|E(\omega_0)|^2}{|E_0(\omega_0)|^2}\,\boldsymbol{da}\right)\cdot\frac{\sum_\theta E^2(\lambda,\theta)}{\sum_\theta E_0^2(\lambda,\theta)} \qquad (4)$$

In addition to the strong enhancement of the local electromagnetic fields and optical density of states, other mechanisms can contribute to the increase of the Raman signal. If the analyte is in physical contact with the metal nanostructure, one must consider the possibility of chemical enhancement resulting from charge transfer between the metal and the molecule.[44] Chemical enhancement contribution is in the range of 10^2-10^3.[45] Additionally, for excitation frequencies close to the absorption bands of a chromophore in the target analyte, the Raman scattering process involves well defined excited energy states of the analyte. This effect, known as Resonant Raman Scattering (RRS), has been shown to enhance Raman signal by a factor of ~10^6.[46] Combining RRS with SERS, overall Raman enhancements of $10^{13\text{-}15}$ were reported.[19]

FDTD optimization

Comprehensive 3D FDTD calculations were performed to explore both the near-field and far-field behaviour of the nano-gaps formed between a spherical silver nanoparticle of diameter D, and an extended silver film, of thickness 100 nm, separated by a gap of width 5 nm (Figure 1). This allowed to probe the influence of key parameters, such as particle diameter D, on the field distribution and enhancements as a function of wavelength.

In the first instance, the extinction spectra of the nano-gaps enable to identify the spectral position of the modes sustained by the nano-gap system. The calculated extinction spectra as a function of particle diameter D (Figure 2(a)) illustrate that hybridized nano-gap systems are fundamentally different from single nanoparticles (second panel of Figure 2(a)). Two extinction maxima, corresponding to two different spectral regions, can be identified in the extinction spectra of the hybridized nano-gap system. Both peaks shift to longer wavelengths as the particle size is increased (Figure 2(b)) illustrating the spectral tunability of the system. By analyzing the charge distributions of the hybridized nano-gap system for each mode (Figure 2(c) and Figure 2(d)), the first extinction peak at shorter wavelengths, can be attributed to the hybridized quadrupolar mode of the coupled system, and the second peak, at longer wavelengths, as its dipolar mode. Correspondingly, the first extinction peak can be shown to be dominated by absorption for D < 100nm and by scattering for D > 100nm, whereas the second extinction peak corresponds mainly to scattering (Figure S1).

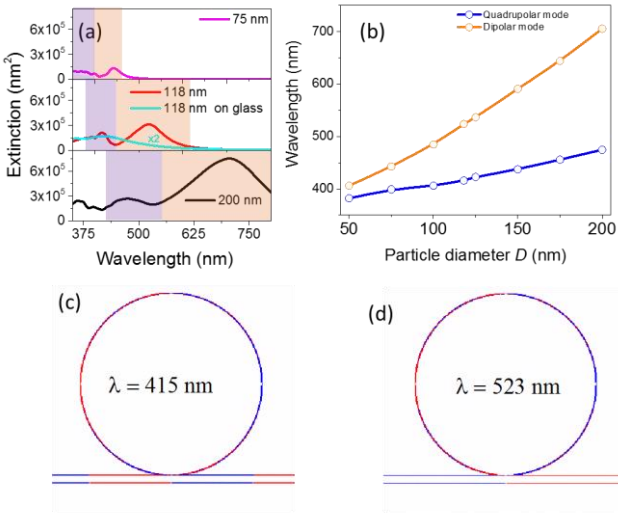

Fig. 2: (a) Calculated extinction spectra as a function of wavelength for a gap of width 5 nm for a silver particle of diameter $\boldsymbol{D}$ = 60 nm, 118 nm and 200 nm respectively. For comparison, the extinction spectrum for a 118 nm particle on a glass substrate is also plotted. (b) Spectral position of the quadrupolar mode and dipolar mode as a function of the silver particle size. (c) and (d) show the charge distribution of the quadrupolar mode and dipolar mode of 118 nm particle size gap respectively.

The spatial distribution of the field enhancement, $|E|/|E_0|$, in the x-z and x-y planes for both the quadrupolar and dipolar modes is almost size independent as can be seen in Figure S2. Both modes correspond to strong field enhancement localized within the nano-gap region indicating that either can be used for SERS application. Additionally, the near-field intensity distributions clearly illustrate the need to use the spatially integrated excitation enhancement $\langle G_{ex} \rangle$, rather than just the maximum excitation intensity G_{ex}, when considering the SERS cross section of low concentration analyte in the nano-gaps, as discussed above.

The optical properties of the nano-gaps were further investigated under focused illumination, using a numerical aperture of 0.55, consistent with the experimental set-up used in this work. Figure 3(a) shows the resulting excitation enhancement factor $\langle G_{ex} \rangle$ as a function of wavelength for a nano-gap with a particle of diameter 118 nm. Under those illumination conditions, the excitation enhancement factor $\langle G_{ex} \rangle$ still presents two regions of enhancement maxima, corresponding to the hybridized quadrupolar and dipolar modes of the system identified earlier (Figure 2(a)). Maximum excitation enhancement is observed for the quadrupolar mode, with an enhancement factor of 3.6×10^2, nearly 2.6 times larger than the maximum excitation enhancement for the dipolar mode (Figure

3(a)). However, this enhancement is purely in the excitation driving the Raman dipole moments in the molecules. In order to quantify the signal detected in the far-field, the emission enhancement factor G_{em} of the plasmonic gap must be taken into consideration. Whereas the excitation enhancement is higher for the multipolar mode (Figure 3(a)), the emission enhancement G_{em} of the system is nearly 12 times larger for the hybridized dipolar mode than for the hybridized quadrupolar mode (Figure 3(b)) as expected.[47] These results highlight the origin of the detected SERS signal as the convolution of the near-field excitation enhancement and the far-field emission enhancement of the plasmonic nano-gap.

Correspondingly, despite the higher excitation enhancement in the near-field for the multipolar mode, when taking into account the emission enhancement in the far-field (Figures 3(b-c)) the dipolar mode is 6 times more efficient than the quadrupolar mode for Raman processes. Additionally, nearly 60% of the enhanced Raman signal corresponding to the dipolar mode of the system is scattered within a cone angle of numerical aperture NA = 0.55 (Figure 3(d)), making it compatible with standard configurations using dry microscope objectives.

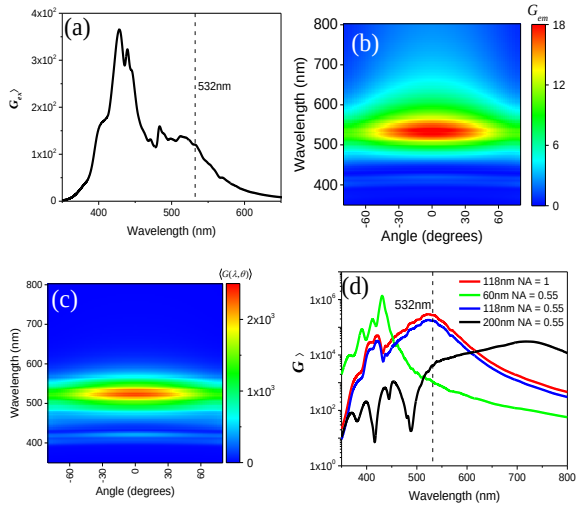

Fig. 3: (a) Calculated near field enhancement factor $\langle \boldsymbol{G_{ex}} \rangle$ for a 5 nm nano-gap formed between a 118 nm silver particle and a 100 nm extended silver film. (b) Calculated emission enhancement factor $\boldsymbol{G_{em}}$ for the same nano-gap. (c) Calculated Raman enhancement $\langle \boldsymbol{G(\lambda, \theta)} \rangle$ for the same nano-gap. (d) Calculated Raman enhancement $\langle \boldsymbol{G(\lambda)} \rangle$ for NA = 0.55, for a 5 nm nano-gap of different particle size 60 nm, 118 nm and 200 nm. For comparison, $\langle \boldsymbol{G(\lambda)} \rangle$ integrated over NA = 1 for the 118 nm particle nano-gap is also presented.

The Raman enhancement $\langle G(\lambda) \rangle$ integrated over a numerical aperture NA = 0.55 was compared for nano-gaps with three different nanoparticle sizes (Figure 3(d)), 60 nm, 118 nm and 200 nm, in order to highlight the impact of the particle size onto the complex interplay between the near-field excitation contribution $\langle G_{ex} \rangle$ and the far-field emission enhancement of the system. The calculated $\langle G(\lambda) \rangle$ for nano-gaps formed with a 60 nm diameter particle is about 7 times higher than $\langle G(\lambda) \rangle$ for nano-gaps formed with a 118 nm particle and 43 times higher than the calculated $\langle G(\lambda) \rangle$ for nano-gaps formed with a 200 nm particle. Despite the fact that the value of $\langle G(\lambda) \rangle$ for the 60 nm particle nano-gap is around 7 times higher than the value of $\langle G(\lambda) \rangle$ for the 118 nm nano-gap, these enhancements are limited to a narrow Raman bandwidth of 700 cm^{-1} compared to the 118 nm particle nano-gap (see Figure S3).

The necessity to have both near-field excitation enhancement at the analyte position to drive the Raman scattering and a high emission enhancement over broad Raman bandwidth to detect all Raman modes in the far field means that, for the systems studied here, the nano-gaps formed with a 118 nm diameter nanoparticle exhibit the optimum figure of merit for Raman enhancement.

Experimental SERS enhancement

To corroborate the FDTD simulations in Figure 3 with experimental measurements, plasmonic nano-gaps of 5 nm were prepared using three different particle sizes: 60 nm, 118 nm and 200 nm. The nano-gaps were doped with the molecular dye Rhodamine 6G at a concentration of 2×10^{-6} M. An excitation wavelength of 532 nm was used in this work, therefore taking advantage of RRS conditions for Rhodamine 6G. SERS spectra were measured from each individual nano-gap and compared to the SERS spectrum measured from off the nano-gap (Figure 4). Each spectrum presented corresponds to the average of measurements from 10 identical structures.

The SERS signal from the 60 nm and 200 nm particle size gaps is found to be very close to the SERS signal measured from off nano-gap, showing a correspondingly low Raman enhancement (Figure 4(a,c)), with the 200 nm particle size nano-gap displaying slightly better efficiency. Conversely, the SERS signal from the 118 nm particle size nano-gap is strongly enhanced and the well-known Raman signal from Rhodamine 6G can be identified. On average, it was found that

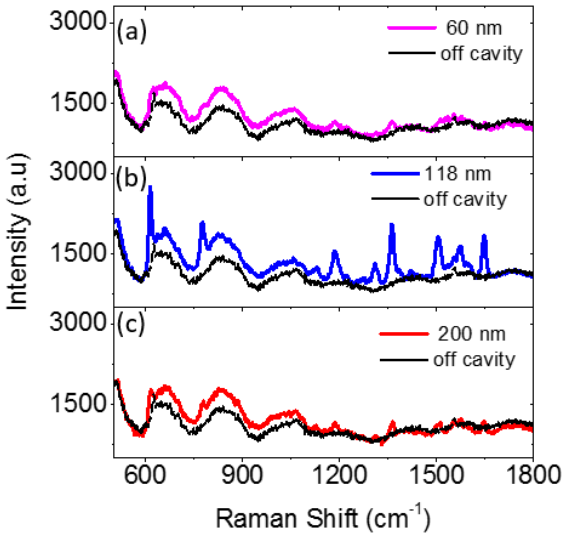

Fig. 4: SERS spectra measured from a 5 nm nano-gap doped with the molecular dye Rhodamine 6G at a concentration of 2×10^{-6} M. In (a) the gap is formed between a 60 nm silver particle and a 100 thick silver film, in (b) the gap is formed between a 118 nm silver particle and a 100 thick silver film and in (c) the gap is formed between a 200 nm silver particle and a 100 thick silver film. For comparison we also plot the measured SERS from off nano-gap regions.

the SERRS signal from the 118 nm particle size nano-gap is four times stronger than the 200 nm particle size nano-gap, in agreement with the FDTD calculations presented in Figure 3(d), for which this enhancement was predicted to be about 7 times at an excitation wavelength of 532 nm.

Single molecule SERS and molecular orientation retrieval

When approaching the single molecule regime, the random orientation of the analytes is no longer averaged over many molecules and the orientation of the Raman active dipoles with respect to the enhanced electric field must be taken into account (see the S_μ term in Eq. 1). Due to the random orientation of molecules, at high concentrations the contribution of the analyte orientation averages to around 1, leading to the full fingerprint spectrum of the material being observed. However, when concentrations drop to sufficiently low values, this averaging disappears and only the modes for which the Raman dipole aligns with the enhanced electric field are expected to be observed in the SERS signal, depending on the molecular orientation relative to the nano-gap field.[13] SERS spectra of Rhodamine 6G at two different concentrations (2×10^{-7} M and 5×10^{-5} M) were measured from a series of optimized nano-gaps with a particle size of 118 nm. At high concentration the SERS signal reproduces the expected Raman signal of Rhodamine 6G,[48] corresponding to the averaging of the analyte orientation in the nano-gap (panel 4 in Figure 5(a)). At the low concentration of 2×10^{-7} M however, differences in the relative intensities of the SERS peaks can be observed between spectra taken over individual nano-gaps (panel 1-3 in Figure 5(a)), suggesting single molecule regime with changes in the molecular orientation from one gap to another. For example the intensity of the phenyl-xanthene in-plane ring-stretching mode (at 621 cm^{-1}; see Figure S5) and the xanthene in-plane ring-stretching mode (at 778 cm^{-1} see Figure S5) have greatly diminished in panel 1 whereas the modes at longer Raman shifts are still observed.

It is important to note that in the systems investigated here, the observed differences in the relative intensities of the SERS peaks from one molecule to another cannot be attributed to Raman photo-bleaching,[49] or to blinking as a result of photo-induced chemical process in the close proximity of the metal surface.[50] To further confirm this, 10 consecutive SERS measurements were taken from the same single molecule over a period of 30 s (Figure 5(c)) showing that the SERS signal remains stable over relativity long periods of time, therefore proving that the observed relative intensity changes in Figure 5(a) are due to changes in molecular orientation from one gap to another.

To retrieve the orientation of the single analyte molecule within the nano-gap, DFT calculations are used to determine the direction of Raman dipole moments for the experimentally observed Raman lines in Figure 5(a) (see table S1 and Figure S4). As can be seen from table S1 the dipole moment associated with the 1647 cm^{-1} Raman line is in the γ direction, while the dipole moments associated with all other Raman lines lay in the α–β plane. Using these two criteria the direction of the nano-gap field relative to the molecular axes α, β and γ can be determined. This analysis indicated that the nano-gap field is predominantly lays in the α–γ plane for molecule 1, in the α–β plane for molecule 2 and equally split between the α–β plane and the α–γ plane for molecule 3 as illustrated in Figure 5(b).

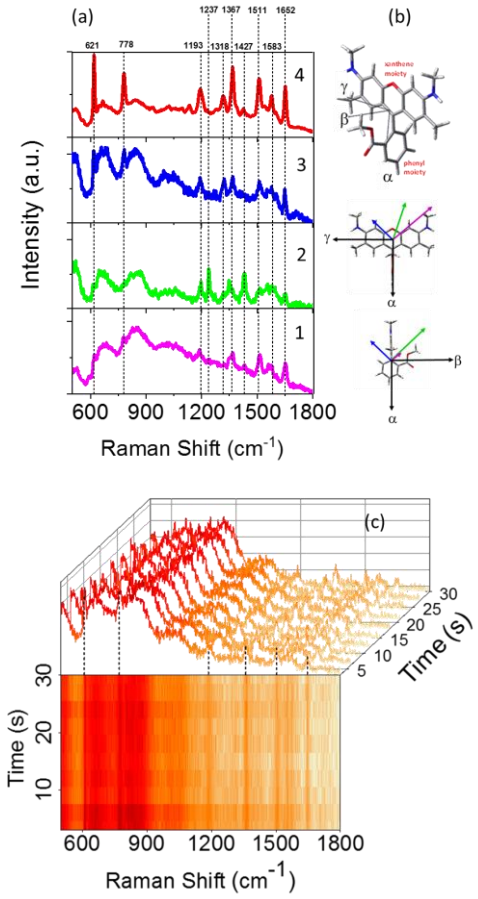

Fig. 5: (a) Spectra 1-3 show three typical single molecule Rhodamine 6G SERS spectra recorded from three different 5 nm nano-gaps formed between a 118nm silver particle and a 100 nm extended silver film. For comparison we plot in panel 4 a high concentration (5×10^{-5} M) SERS spectrum of Rh6G. (b) Top part: Rhodamine 6G molecule with main moieties indicated. Bottom part: the projection of the nano-gap field on molecules 1, 2 and 3 in α–γ and α–β planes. (c) Time dependent single molecule SERS spectra (accumulation time 3 s, total time 30 s).

Conclusions

In summary, we have demonstrated numerically and experimentally an optimized plasmonic nano-gap with single molecule detection capability. SERS measurements and FDTD modelling show that the SERS signal from the investigated nano-gaps is strongly dependent on the particle size and the molecular orientation. This behavior is attributed to the complex interplay between the near-field excitation enhancement and the far-field emission enhancement for

various particle size nano-gaps. Concentration dependent SERS measurements and time dependent SERS measurements provide clear evidence that our optimized nano-gaps are able to suppress blinking, thus leading to a reliable and stable single molecule detection protocol. Through combining the results of our DFT and FDTD calculations the molecular orientation within the plasmonic nano-gap is recovered. The ability to determine the molecular orientation combined with methods to control the molecular orientation during the fabrication/synthesis stages will have a profound impact on different fields ranging from molecular electronic devices to biomedical applications.

Acknowledgements

We thank the University of Hull for the PhD scholarships which funded this project. This work was partially supported by the UK EPSRC through Grant. No. EP/L025078/1 "Self assembly of two dimensional colloidal alloys for metamaterials applications" and the European COST Action Nano-spectroscopy, MP1302. The work at IMDEA was supported by the Spanish Ministerio de Economıá y Competitividad (MINECO-FEDER project CTQ2014-58801) and by the Cam-pus of International Excellence (CEI) UAM+CSIC. We thank Stuart Harris at Zeon Chemicals Europe Ltd. For the gift of the Zeonex polymer)

Notes and references

[1] K. B. Crozier, W. Zhu, D. Wang, S. Lin, M. D. Best, and J. P. Camden, *IEEE J. Sel. Top. Quantum Electron.*, **2014**, 20, 3, 1–11.

[2] H. A. Atwater and A. Polman, *Nat. Publ. Gr.*, **2010**, 9, 3, 205–213.

[3] K. Hong and J. Lee, *Electron. Mater. Lett.*, **2011**, 7, 2, 77–91.

[4] R. Zia, J. A. Schuller, A. Chandran, and M. L. Brongersma, *materialstoday*, **2006**, 9, 7, 20–27.

[5] R. Kirchain and L. Kimerling, *Nat. Photonics*, **2007**, 1, 303–305.

[6] P. P. Maharjan *et al.*, *Phys. Chem. Chem. Phys.*, **2013**, 15, 18, 6856–6863.

[7] S. A. Maier, *PLASMONICS: FUNDAMENTALS AND APPLICATIONS*, 1st ed. Bath: Springer, **2007**.

[8] Heinz Raether, *Surface Plasmons on Smooth and Rough Surfaces and on Gratings*, 1st ed., 111. Berlin: Springer Berlin Heidelberg, **1988**.

[9] K. Kneipp *et al.*, *Phys. Rev. Lett.*, **1997**, 78, 9, 1667–1670.

[10] P. G. Etchegoin, E. C. Le Ru, and A. Fainstein, *Phys. Chem. Chem. Phys.*, **2011**, 13, 10, 4500–4506.

[11] E. C. Le Ru, M. Meyer, and P. G. Etchegoin, *J. Phys. Chem. B*, **2006**, 110, 4, 1944–1948.

[12] H. M. Lee, S. M. Jin, H. M. Kim, and Y. D. Suh, *Phys. Chem. Chem. Phys.*, **2013**, 15, 15, 5276–5287.

[13] R. Zhang *et al.*, *Nature*, **2013**, 498, 7452, 82–6.

[14] S. Nie, *Science*, **1997**, 275, 5303, 1102–1106.

[15] C. V. Raman and K. S. Krishnan, *Nature*, **1928**, 121, 3048, 501–502.

[16] K. Kneipp and H. Kneipp, *Focal point*, **2006**, 60, 12, 322–334.

[17] K. Kneipp, *Phys. Today*, **2007**, 60, 11, 40–46.

[18] E. C. Le Ru, E. Blackie, M. Meyer, and P. G. Etchegoin, *J. Phys. Chem. C*, **2007**, 111, 13794–13803.

[19] T. Itoh and Y. S. Yamamoto, *Analyst*, **2016**, 141, 17, 5000–5009.

[20] H. Günzler and H.-U. Gremlich, *Handbook of spectroscopy*, 2nd ed. Germany: Wiley-VCH, **2003**.

[21] P. G. Etchegoin and E. C. Le Ru, *Phys. Chem. Chem. Phys.*, **2008**, 10, 40, 6079–6089.

[22] P. J. G. Goulet and R. F. Aroca, *Anal. Chem.*, **2007**, 79, 7, 2728–2734.

[23] Y. Wang and J. Irudayaraj, *Philos. Trans. R. Soc. Lond. B. Biol. Sci.*, **2013**, 368, 1611, 1–10.

[24] M. Pelton and G. Bryant, *Introduction to Metal-Nanoparticle Plasmonics*, 1st ed. New Jersey: Wiley-Blackwell, **2013**.

[25] C. Ciracì *et al.*, *Science*, **2012**, 337, 1072–4.

[26] S.-Y. Ding, J. Yi, J.-F. Li, B. Ren, R. Panneerselvam, and Z.-Q. Tian, *Nat. Rev.*, **2016**, 1, 16021, 1–16.

[27] Z. Jin, W. Gu, X. Shi, Z. Wang, and Z. Jiang, *Adv. Opt. Mater.*, **2014**, 2, 6, 1–9.

[28] D. Lim, K. Jeon, H. M. Kim, J. Nam, and Y. D. Suh, *Nat. Mater.*, **2009**, 9, 1, 60–67.

[29] Y. Fang and Y. Huang, *Appl. Phys. Lett.*, **2013**, 102, 153108, 1–5.

[30] J.-M. Nam, J.-W. Oh, H. Lee, and Y. D. Suh, *Acc. Chem. Res.*, **2016**, 49, 2746–2755.

[31] M. Moskovits, *Nano Lett.*, **2012**, 12, 2088–2094.

[32] Y. Huang, L. Ma, M. Hou, J. Li, Z. Xie, and Z. Zhang, *Sci. Rep.*, **2016**, 6, 1, 1–9.

[33] R. W. Taylor *et al.*, *Sci. Rep.*, **2014**, 4, 5940, 1–6.

[34] X. Wang *et al.*, *ACS Nano*, **2014**, 8, 1, 528–536.

[35] D. O. Sigle *et al.*, *J. Phys. Chem. Lett.*, **2016**, 7, 4, 704–710.

[36] A. Lombardi *et al.*, *ACS Photonics*, **2016**, 3, 3, 471–477.

[37] J. N. Anker, W. P. Hall, O. Lyandres, N. C. Shah, J. Zhao, and R. P. Van Duyne, *Nat. Mater.*, **2008**, 7, 6, 442–453.

[38] R. T. Hill *et al.*, *Nano Lett.*, **2010**, 10, 10, 4150–4154.

[39] M. Hu, A. Ghoshal, M. Marquez, and P. G. Kik, *J. Phys. Chem.*, **2010**, 114, 7509–7514.

[40] L. Li, T. Hutter, U. Steiner, and S. Mahajan, *Analyst*, **2013**, 138, 16, 4574–4578.

[41] P. Johnson and R. Christy, *Phys. Rev. B - Condens. Matter Mater. Phys.*, **1972**, 6, 12, 4370–4379.

[42] M. J. Frisch, "Gaussian 09," *Gaussian 09*. Gaussian, Inc., 2009.

[43] F. J. Garcı and J. B. Pendry, *Phys. Rev. Lett.*, **1996**, 77, 6, 1163–1166.

[44] Z. Wang and L. J. Rothberg, *J. Phys. Chem.*, **2005**, 8, 109, 3387–3391.

[45] S. D. Hudson, G. Chumanov, H. L. H. Laboratories, and S. Carolina, *J. Chem. C*, **2008**, 112, 19866–19871.

[46] E. C. Le Ru and P. G. Etchegoin, *Principles of Surface Enhanced Raman Spectroscopy and related plasmonic effects*. **2009**.

[47] A. P. Edwards, A. M. Adawi, A. P. Edwards, and A. M. Adawi, *J. Appl. Phys.*, **2014**, 115, 5, 1–7.

[48] X. N. He *et al.*, *Nanotechnology*, **2012**, 23, 20, 205702.
[49] R. C. Maher, L. F. Cohen, and P. Etchegoin, *Chem. Phys. Lett.*, **2002**, 352, 378–384.
[50] K. L. Kelly, E. Coronado, L. L. Zhao, and G. C. Schatz, *J. Phys. Chem. B*, **2003**, 107, 3, 668–677.